Proteomics of the Retinal Pigment Epithelium Reveals Altered Protein Expression at Progressive Stages of Age-Related Macular Degeneration

Curtis L. Nordgaard,[1,2] *Kristin M. Berg,*[1,2] *Rebecca J. Kapphahn,*[1] *Cavan Reilly,*[3] *Xiao Feng,*[1] *Timothy W. Olsen,*[1] *and Deborah A. Ferrington*[1]

Purpose. Age-related macular degeneration (AMD) is characterized clinically by changes in the retinal pigment epithelium (RPE), formation of drusen between the RPE and the underlying vasculature, geographic atrophy, and choroidal neovascularization. Later clinical stages are accompanied by impaired central vision. A limited understanding of the molecular events responsible for AMD has constrained the development of effective treatments. A proteomics approach was used to investigate the underlying mechanisms of AMD and to identify proteins exhibiting significant changes in expression with disease onset and progression.

Methods. Human donor eyes were categorized into one of four progressive stages of AMD. Proteins from the RPE were resolved and quantified by two-dimensional (2-D) gel electrophoresis. Proteins exhibiting significant expression changes at different disease stages were identified by matrix-assisted laser desorption ionization time-of-flight (MALDI-TOF) mass spectrometry. 2-D and semiquantitative one dimensional (1-D) Western blot analyses were used to determine whether changes identified by the proteomic analysis were specific for a protein subpopulation or representative of the entire protein population.

Results. Proteins were identified from several critical pathways that changed at early and late disease stages, indicating potential causal mechanisms and secondary consequences of AMD, respectively. Proteins involved in protecting from stress-induced protein unfolding and aggregation, mitochondrial trafficking and refolding, and regulating apoptosis changed early in the disease process. Late-stage changes occurred in proteins that regulate retinoic acid and regeneration of the rhodopsin chromophore.

Conclusions. These results provide the first direct evidence of AMD stage-specific changes in human RPE protein expression and provide a basis for functional investigation of AMD that may ultimately suggest new therapeutic strategies. (*Invest Ophthalmol Vis Sci.* 2006;47:815–822) DOI:10.1167/iovs.05-0976

Age-related macular degeneration (AMD) is the leading cause of vision loss and blindness in individuals older than 65 years in the developed world.[1,2] Epidemiologic studies have shown that approximately 10% of individuals older than 65 years and 28% of those aged 75 to 85 years have features of AMD.[1] According to statistics from the U.S. census, nearly 10 million more U.S. citizens will enter the 65+ demographic in the next 20 years,[3] thus qualifying AMD as an impending public health epidemic. Clinically, AMD manifests as changes in the retinal pigment epithelium (RPE), a monolayer of cells that lie between the photoreceptors and Bruch's membrane, separating the photoreceptors from the highly vascular choroid. Maintenance of RPE function is essential for vision, since these cells serve as a conduit for nutrients from the choroid to the retina, recycle visual pigments, and phagocytose spent photoreceptor outer segments.[4] Early AMD is characterized by the appearance of lipoproteinaceous deposits (drusen) between the RPE and choroid, as well as changes in RPE pigmentation. Later stages of AMD accompanied by vision loss are characterized by increased drusen accumulation, RPE atrophy, choroidal neovascularization, and loss of photoreceptors.[5–7] Unfortunately, current treatments for this disease are constrained by our limited understanding of the molecular events associated with AMD. Clarification of the mechanisms responsible for AMD onset and progression is critical for developing treatments to prevent late AMD and, hence, preserving visual function in an aging population.

Several pathogenic mechanisms have been proposed to explain the complex etiology of AMD, including RPE cell death,[8] oxidative damage of cellular components,[9] mitochondrial dysfunction,[10] and the accumulation of toxic compounds, such as lipofuscin and advanced glycation end products.[11,12] In addition, inflammation and activation of the innate immune system probably contribute to the pathogenesis of AMD, since drusen contain proinflammatory molecules,[13–15] and complement factor H (*HF1/CFH*) genetic polymorphisms correlate with the disease in a subset of patients with AMD.[16–19] However, the molecular events that mediate these pathogenic mechanisms must be more clearly defined to facilitate the development of targeted therapies for AMD.

We have applied a proteomic experimental strategy to investigate global RPE protein expression changes that correlate with AMD onset and progression. Human donor eyes were categorized into one of four progressive stages of AMD using the Minnesota Grading System (MGS).[7] The MGS was recently developed based on criteria from the Age-Related Eye Disease Study (AREDS),[20] considered to be the standard in clinical and epidemiologic studies of AMD. Two-dimensional (2-D) and

From the [1]Department of Ophthalmology and the [3]Division of Biostatistics, University of Minnesota, Minneapolis, Minnesota.

[2]Contributed equally to the work and therefore should be considered equivalent authors.

Supported in part by National Eye Institute Grant EY014176 (DAF), National Institute on Aging Grant AG025392 (TWO), a Career Development Award from the American Federation for Aging Research and Foundation Fighting Blindness (DAF), the American Health Assistance Foundation, the Minnesota Medical Foundation, the University of Minnesota Academic Health Center and Graduate School, the Fesler-Lampert Foundation, an Undergraduate Research Opportunities award (KMB) from the University of Minnesota, and an unrestricted grant to the Department of Ophthalmology from the Research to Prevent Blindness Foundation.

Submitted for publication July 26, 2005; revised October 13, 2005; accepted January 6, 2006.

Disclosure: **C.L. Nordgaard,** None; **K.M. Berg,** None; **R.J. Kapphahn,** None; **C. Reilly**, None; **X. Feng**, None; **T.W. Olsen,** None; **D.A. Ferrington**, None

The publication costs of this article were defrayed in part by page charge payment. This article must therefore be marked "*advertisement*" in accordance with 18 U.S.C. §1734 solely to indicate this fact.

Corresponding author: Deborah A. Ferrington, 380 Lions Research Building, 2001 6th Street SE, Minneapolis, MN 55455; ferri013@umn.edu.

semi-quantitative one-dimensional (1-D) Western blot analyses provided further insight into whether the changes identified by proteomics were specific for a protein subpopulation or representative of the entire protein population. By using comparative proteomics to examine human donor tissue graded by using the MGS, we provide direct evidence for specific changes in the expression of RPE proteins and, most important, changes at the earliest stages of AMD.

METHODS

Human Tissue Procurement and Grading

Donor eyes were obtained from the Minnesota Lions Eye Bank and maintained at 4°C in a moist chamber until dissection and photography. All tissue was acquired with the consent of the donor or the donor's family for use in medical research in accordance with the principles outlined in the Declaration of Helsinki. Eyes were graded for the presence and severity of AMD using the MGS.[7] One eye from each pair was immediately frozen in liquid nitrogen and stored at −80°C for subsequent biochemical analyses. The neurosensory retina from the second eye of each pair was dissected to expose the RPE. Digital photographs of the RPE were then used to identify the clinical features that distinguish each stage of AMD.

Protein Isolation

Globe dissection proceeded as outlined.[21] After removing the neurosensory retina and the macula with an 8-mm trephine punch, the RPE was moistened with calcium and magnesium-free phosphate-buffered saline and gently abraded to dislodge it from the choroid. RPE cells were pelleted by centrifugation at 1100*g* for 30 minutes and fractionated in 50 mM Tris (pH 7.8) with 2% CHAPS (3-[3-cholamidopropyl]dimethylammonio-2-hydroxy-1-propanesulfonate) by three freeze-thaw cycles and mechanical homogenization at 4°C. Lysates were centrifuged at 600*g* for 15 minutes at 4°C to pellet cell debris. After removal of lipids and nucleic acids by acetone precipitation, samples were resuspended in 8 M urea and 0.5% CHAPS. Protein concentration was measured with the bicinchoninic acid assay (Pierce Biotechnology, Rockford, IL), with bovine serum albumin used as the protein standard.

Photoreceptor Outer Segment Isolation

Human RPE cells were harvested as just described. One-third of each sample was used for RPE fractionation and protein quantification. The remaining two thirds were pelleted as described in the prior section, resuspended in phosphate-buffered saline, and loaded onto a continuous sucrose gradient for outer segment purification as described.[21] Total photoreceptor outer segment protein yield was calculated as a percentage of the total protein yield from that sample. Three to four preparations were analyzed for each MGS stage.

2-D SDS-PAGE and Expression Analysis

2-D sodium dodecyl sulfate polyacrylamide gel electrophoresis (SDS-PAGE) was performed[22] with 140 μg of RPE protein. The first dimension separation was performed on pH-5 to -8 immobilized linear gradient strips (Bio-Rad, Hercules, CA) and second-dimension separation on 12% SDS-polyacrylamide gels (14 × 16 cm).[23] After electrophoresis, gels were stained silver with a mass spectrometry-compatible kit (Silver Stain Plus Kit; Bio-Rad) and imaged with a fluorescence imager (Fluor-S Multi-Imager; Bio-Rad). Spot intensities (spot volume) were quantified by computer (PDQuest 7.1.1; Bio-Rad). This program performs gel-to-gel comparisons by using algorithms that account for differences in background and staining intensities. Gel-to-gel spot matching was performed by generating a master gel and manually selecting 12 spots that were consistently present in all gels as landmarks. Automatic spot detection was followed by manual inspection and spot editing to ensure consistent matches between gels. Statistical analyses were performed with $\log_2$-transformed spot intensities.

Protein Identification

Spots that exhibited significant changes in intensity were excised from 2-D polyacrylamide gels and processed for mass spectrometry (MS).[22] Matrix-assisted laser desorption ionization time-of-flight (MALDI-TOF) MS was performed to obtain peptide mass fingerprints (QSTAR XL quadrupole-TOF mass spectrometer; Applied Biosystems Inc. [ABI], Foster City, CA), as described.[22] Peptide peaks identified on computer (Bioanalyst; ABI) were submitted to Mascot (www.matrixscience.com/; Matrix Science, Inc., Boston, MA) to obtain an initial protein identification. Positive identification was based on a significant molecular weight search (MOWSE) score and mass tolerance less than 50 parts per million.

Confirmation of initial identities was obtained by peptide mass sequencing, by using either MALDI or electrospray ionization (ESI) MS. Peptides analyzed by ESI were separated by liquid chromatography online (QSTAR Pulsar quadrupole TOF; ABI) and ionized as described.[22] PROID software was used to identify peptides based on the product ion spectra.

Western Immunoblot Analysis

Resolution of RPE proteins by 1-D or 2-D SDS-PAGE and Western immunoblot analysis was performed as described.[21,22] Blotted proteins were probed with one of the following primary antibodies: glutathione *S*-transferase π (GST-π; CalBiochem-Novobiochem, La Jolla, CA), ATP synthase β (BD PharMingen, San Diego, CA), cellular retinaldehyde binding protein (CRALBP; gift from John Saari, University of Washington); mitochondrial heat shock protein (HSP)-75 (mtHSP75; StressGen, San Diego, CA), HSP60 (BD Biosciences, Franklin Lakes, NJ), cellular retinoic acid binding protein-1 (CRABP1; Sigma-Aldrich, St. Louis, MO), αA crystallin (StressGen), and voltage-dependent anion channel-1 (VDAC1; CalBiochem). Goat anti-mouse or rabbit secondary antibodies (Bio-Rad) conjugated to alkaline phosphatase were used in conjunction with the substrate 5-bromo-4-chlor-3′-iodolyl phosphate *p*-toluidine/nitro blue tetrazolium chloride to visualize immune reactions. Membranes were imaged with the fluorescence imager (Fluor-S Multi-Imager; Bio-Rad), followed by quantification (Scan Pro; Sigma-Aldrich).[21]

Statistical Analysis

A power analysis was performed with the equation in Ferrington et al.,[24] to determine the number of samples needed to detect statistically significant differences between groups. The analysis was based on within-group variation in the intensity of individual spots from 2-D gels.

To test for differences in spot intensities between disease stages, we used a mixture model analysis of variance (ANOVA), which extends the usual ANOVA to allow for the presence of zeros in the data. The mixture model supposes that for each disease stage there is a certain probability of observing a zero and if nonzero, then the observation is normally distributed with some mean response. Thus, each group is characterized by two parameters: a probability of zero and a mean level for the nonzero responses. We then used a maximized likelihood-ratio test,[25] to test the hypothesis that the probability of observing zero or the mean level of the nonzero cases differs between groups.

One-way ANOVA was performed on density measurements of 1-D blot immune reactions, and times from death to enucleation, and from enucleation to freezing. Linear regression analysis was performed to compare spot density with time from death to freezing. Statistical significance was determined by $P \leq 0.05$.

RESULTS

Description of Experimental System

Table 1 summarizes the demographic and clinical donor information obtained from the Minnesota Lions Eye Bank. Donors

TABLE 1. Donor Demographics and Clinical Information

MGS Grade	Sample Size* (*n*) Total	F	M	Smoking History† (*n*)	Age‡ (y)	Age Range (y)	Cause of Death§
1	7	2	6	3	58 ± 12	37–71	Stroke (1), heart disease (2), cancer (4), pneumonia (1)
2	7	6	4	2	66 ± 7	57–75	Stroke (1), heart disease (1), cancer (4), pneumonia (1), head trauma (1), necrotic bowel (1)
3	7	2	7	2	73 ± 8	59–86	Heart disease (3), cancer (1), age (1), sepsis (1), renal failure (1), anoxic brain injury (1), pulmonary edema (1)
4	7	3	6	5	80 ± 10	71–94	Stroke (1), heart disease (3), respiratory failure (2), pneumonia (1), age (1), acute cardiac event (1)

* Some samples from the same grade were combined.
† Number of donors with a positive smoking history.
‡ Mean ± SD; § Number of donors in each category is indicated in parentheses.

with a known history of diabetes or eye disease other than age-related macular degeneration were excluded from the study. Only white donors were used, because of the differences in AMD prevalence among individuals with light or dark pigmentation.[26] The average time from death to enucleation was 5.1 ± 0.5 hours (mean ± SD). Eyes were maintained at 4°C until they were photographed and frozen for proteomic analysis. Average time from enucleation to freezing was 12.1 ± 4.6 hours. There were no significant differences in time to enucleation or freezing between the four MGS groups.

The MGS[7] was used to classify donor eyes into four progressive stages (referred to as MGS-1 to -4) that correspond to the classification of AMD described in the AREDS report.[20] MGS stages are defined primarily by the number and size of yellow deposits (drusen), RPE changes, atrophic areas of the RPE, and the presence of neovascularization. MGS stage 1 serves as the control and includes individuals with few, small drusen. MGS 2 is considered an early stage of AMD (i.e., having more numerous small drusen and pigmentary changes than MGS 1 but without significant vision-related degeneration). The most clinically relevant change in prognosis for future vision loss occurs from AREDS 2 to 3, or corresponding MGS 2 to 3. MGS 3 is defined by numerous intermediate-sized drusen or noncentrally located geographic atrophy. Advanced AMD (MGS 4) corresponds with central vision loss from geographic atrophy, also known as atrophic AMD, or active choroidal neovascularization, also known as exudative (e)AMD. This occurs when neovascularization that originates in the choroid extends into the subfoveal region and results in severe progressive fibrosis of the macula. Because the majority (6/7) of MGS4 samples from the present study contained protein from donors classified as eAMD, protein samples were prepared from the extramacular RPE to minimize contamination from macular neovascularization and fibrosis.

Seven samples from each MGS category were analyzed. A power analysis based on the variation in intensity of individual spots from 2-D gels showed this number was adequate to detect a twofold change in intensity at 90% power with $\alpha = 0.05$. A total of 447 spots were clearly resolved and analyzed. Linear regression was performed (spot density versus time from death to freezing) to evaluate the stability of retinal proteins from donor eyes. We found no significant relationship between spot density and time in >95% of the protein spots examined. We interpret these results to indicate that under our experimental conditions, there was no significant time-dependent degradation for the majority of the RPE proteins examined.

To determine the extent of photoreceptor outer segment contamination in our RPE preparations, we quantified the photoreceptor outer segment protein that copurified with the RPE. The average relative contribution of outer segment protein to the total yield was 5.4% ± 1.0% (SEM; $n = 13$). There was no linear relationship between the MGS stage and the percentage of outer segment contamination ($t = 0.82$, $P < 0.43$), suggesting that outer segment contamination in the RPE samples did not vary between MGS stages.

Expression Analysis and Protein Identification

Protein spots resolved by 2-D gel electrophoresis that exhibited a significant change in expression with AMD are indicated in a representative silver-stained gel (Fig. 1). Densitometric analysis of these proteins showed three distinct patterns of

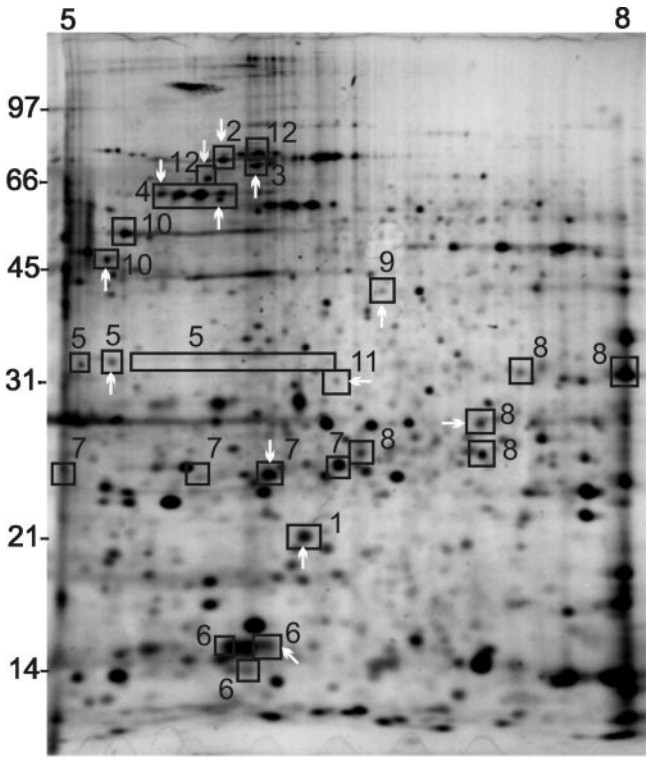

FIGURE 1. Retinal proteins resolved by 2-D gel electrophoresis. Representative silver-stained gel (140 μg) indicates proteins demonstrating altered expression with AMD. Boxed spots were identified by either a positive immune reaction with protein-specific antibodies or by MS. *Arrows*: spots demonstrating altered protein expression. The pH range for first dimensional separation (pH 5–8) is shown at the *top*. Numbers correspond with the proteins listed in Table 2.

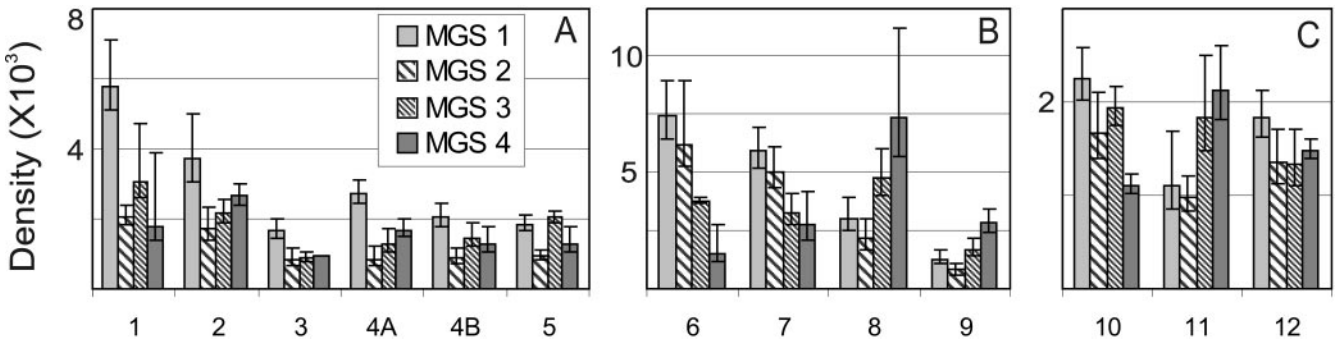

FIGURE 2. Spots showing significant changes in expression with AMD. Results of densitometry for protein spots on 2-D silver-stained gels demonstrating significant changes early in AMD (**A**), a linear increase or decrease (**B**), or at later stages in AMD (**C**). Data are the mean (±SEM) spot densities for each MGS category. Missing data were not included in the calculation of the mean. Asymmetric error bars reflect back-transformation from $\log_2$ values. Numbers correspond with the proteins listed in Table 2.

expression that correspond with changes early (MGS 2) in the disease, linear increases or decreases, and changes in late (MGS 4) AMD (Fig. 2). Initial identification of these proteins was obtained with MALDI-TOF MS and confirmed by either tandem MS sequencing of peptides or by a positive immune reaction on 2-D Western blot analysis with a protein-specific antibody (Table 2). Proteins that resolve into multiple spots on 2-D gels due to posttranslational modifications that alter the native charge are known as charge trains, and each individual spot is referred to as an isoelectric variant. Immune reactions on 2-D Western blot analysis provided an indication of the distribution of spots for each protein and the relative contribution of each isoelectric variant in the population (Fig. 3). When possible, 1-D Western blot analyses were subsequently performed to quantify protein expression in the entire population (Fig. 4).

Six spots demonstrated an early decrease in protein expression (Fig. 2A). MALDI-TOF MS identified five spots of this group as members of the HSP family (HSP60, HSP70, heat shock cognate [HSC]-70, αA crystallin). For HSC70 and HSP70, no additional analyses are presented due to unreliable antibody reactions and antibody cross-reactivity with other members of the HSP family, respectively. 2-D Western blot analysis probing with antibodies to αA crystallin showed a single immunoreactive spot that corresponded with the spot identified by MS (Fig. 3, spot 1). Semiquantitative 1-D Western blot analysis of protein expression for αA crystallin showed a significant decline ($P = 0.006$) in immune reaction at MGS 3 and 4 (Fig. 4). These results are consistent with spot density measurements although the decline in early AMD (MGS 2) was not evident in 1-D analysis.

Probing 2-D Western blots with antibodies to HSP60 (Fig. 3, spot 4) revealed that multiple protein spots were immune reactive. The two spots demonstrating significant early decreases in expression accounted for ~20% of the total population. 1-D Western blot analysis for HSP60 showed no significant change in total protein content when comparing the four levels of MGS (data not shown). These results demonstrate that only a subpopulation of HSP60 changes in AMD.

MALDI-TOF MS analysis of spot 5 indicated a mixture of two proteins: CRALBP and ATP synthase β. Migration of spot 5 was lower than expected for ATP synthase β, indicating that this spot contains truncated protein or a proteolytic fragment. On 2-D Western blot analysis, the antibody that recognizes ATP synthase β did not react with spot 5 (data not shown). The discrepancy between MS identification and antibody recognition could reflect truncated ATP synthase β that is missing the C-terminal epitope recognized by the antibody. Consistent with this idea, no C-terminal peptides were present in the mass fingerprint generated by MALDI-TOF MS. When probing for CRALBP, we observed multiple immunoreactive spots (Fig. 3).

TABLE 2. Protein Identification by Mass Spectrometry and Western Blot Analysis

				MALDI-TOF			
Spot	**Protein**	**Accession No.***	**Theoretical MW/pI†**	**Peptides (*n*)**	**% Coverage**	**MS/MS‡ Peptides (*n*)**	**Western Blot Immune Reaction**
1	αA crystallin	NP_000385	19.9/5.8	9	53	3	+
2	HSC 70	NP_006588	73.0/5.6	16	42	4	
3	HSP 70	NP_005336	70.0/5.5	12	25	4	
4A	HSP 60	NP_002147	61.0/5.7	9	28		+
4B	HSP 60	NP_002147	61.0/5.7	6	17	1	+
5	CRALBP	NP_000317	36.5/5.0	12	44		+
5	ATP synthase β	NP_001677	56.5/5.3	8	41		
6	CRABP I	NP_004369	15.5/5.3	7	51		+
7	GST-π	NP_000843	23.2/5.4	8	52	2	+
8	VDAC 1	NP_003365	30.6/8.6	7	32	2	
9	Pyruvate kinase	NP_002645	57.9/8.0			2	
10	ATP synthase β	NP_001677	56.3/5.3	8	23		+
11	elF4H	NP_071496	31.2/7.7	12	42		
12	mt HSP 75	NP_004125	73.7/6.0	5	10		+

* Accession no. from GenBank, NCBI, Bethesda, MD; http://www.ncbi.nlm.nih.gov/Genbank/.

† Molecular weight in kDa.

‡ Includes peptides sequenced by MALDI-TOF-MS/MS and ESI-MS/MS.

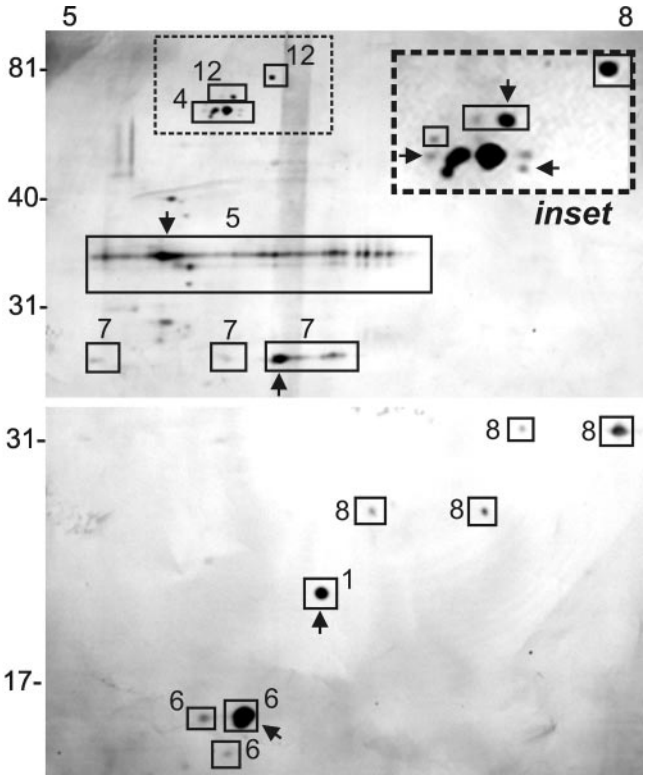

FIGURE 3. Immunereactive spots on 2-D Western immunoblots identify retinal proteins. RPE proteins (140 μg) were resolved by 2-D SDS-PAGE, transferred, and probed with antibodies to specific proteins. Blots were stripped between antibodies and reprobed. *Arrows*: spots with altered expression. *Inset*: enlarged area of staining for HSP60 and mtHSP75 (*boxed*). Numbers correspond with proteins listed in Table 2. Note that staining with an anti-CRALBP antibody accounts for reaction 5.

Whereas spot 5 was part of the CRALBP charge train, its contribution was only a fraction of the total protein population. Densitometry of 1-D Western immune reactions showed a significant increase ($P = 0.006$) in CRALBP content at MGS 3 and 4. These results highlight the importance of examining each protein separately when a mixture of proteins is present in a single spot.

Four spots demonstrated a linear change in protein expression (Fig. 2B) and were identified by MALDI-TOF MS analysis. Spots containing CRABP1 and GST-π showed significant progressive decreases in density. On 2-D Western immunoblots, the antibody to CRABP1 reacted with a large spot that agreed with the MS identification and in addition, two minor spots migrating to become more acidic and at a lower mass than the major spot (Fig. 3, spot 6). Results from 1-D Western blot analysis showed a significant decrease ($P = 0.007$) in CRABP1 at MGS 3 and 4, thus confirming 2-D spot density measures. For GST-π, the MS identified spot was one of several immunoreactive spots on 2-D blots (Fig. 3, spot 7). The spot decreasing in density accounted for ~33% of the total GST-π population. In contrast, the density of the other GST-π immunoreactive spots exhibited a nonsignificant increase with the disease (data not shown). Consistent with the general increase in density on 2-D gels for most of the population, 1-D Western blot analysis showed a significant increase ($P = 0.002$) in expression at MGS 3 and 4. These results demonstrate that specific isoelectric variants can change in content, independent from the major protein population.

Two protein spots demonstrating a linear increase in expression with AMD were identified as VDAC1 and pyruvate kinase. No further analyses were conducted for pyruvate kinase because the antibody reaction was unreliable. Western 2-D blots probing for VDAC1 showed a pair of immune reactive spots at ~31 kDa and a second pair at ~26 kDa (Fig. 3, spot 8). MS analysis confirmed all but the most basic spot that was poorly resolved at ~31 kDa as VDAC1, which is probably the parent protein based on its agreement with the theoretical pI and mass. The acidic isoelectric variant at either 31 or 26 kDa is probably a result of phosphorylation of Ser 103 for this protein.[27] The pair of spots migrating at 26 kDa have mass (25.5 kDa) and pI (6.9 and 6.2) that are consistent with cleavage of ~50 residues from the C terminus. The spot identified by MS positioned at ~28 kDa that demonstrated increased expression with AMD did not react with the antibody. Because the VDAC1 antibody was generated against the N-terminal 19 amino acids, a potential explanation is that VDAC1 in spot 8 lacks the N terminus. The absence of N-terminal peptides in the mass fingerprint generated from this spot is consistent with this explanation. A 1-D Western blot analysis probing for VDAC1 total protein content demonstrated a significant linear decline ($P = 0.007$) with progression of AMD. Examination of the 2-D gel density for the three clearly resolved spots at 31 and 26 kDa showed no significant change with AMD. However, the most basic unresolved spot had the strongest immune reaction, suggesting it made the greatest contribution to the 1-D reaction and therefore is likely responsible for the decrease in VDAC1 expression.

Three spots demonstrated significant changes in density at late stage (MGS-4) AMD (Fig. 2C). MALDI-TOF MS analysis identified these spots as ATP synthase β (spot 10), eukaryotic transcription initiation factor 4H (eIF4H; spot 11), and mtHSP75 (spot 12). No additional data are available for eIF4H, because the antibody is not commercially available. The reaction on 2-D Western blot analysis for ATP synthase β was at a single spot with the expected mass and pI (data not shown). However, the spot changing in expression and identified by MS migrated to be more acidic and ~3 kDa lower than the parent protein, indicating a proteolytic fragment of ATP synthase β. The antibody to ATP synthase β recognizes the C terminus (residues 428-539), so we examined the mass fingerprint generated by MALDI-TOF MS and confirmed that no C-terminal peptides were present in spot 10. One-dimensional Western immunoblots probed with an antibody to ATP synthase β showed no significant change in immune reaction for the parent protein across the four MGS levels (data not shown).

Two major spots and two minor spots reacted with the antibody to mtHSP75 on 2-D Western blot analysis (Fig 3, spot

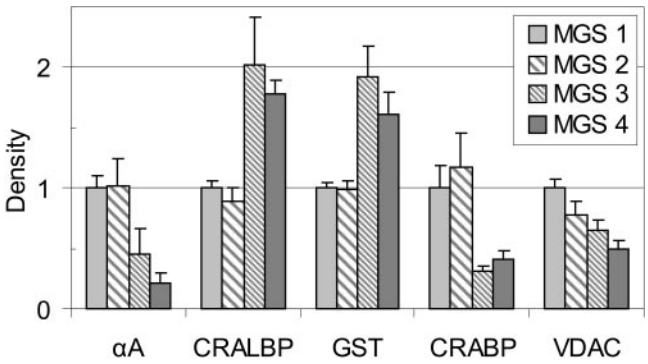

FIGURE 4. Semiquantitative analysis of protein expression by 1-D Western immunoblot analysis. Densitometric analysis of immune reactions for RPE proteins resolved on 1-D gels showed significant ($P < 0.01$ for all comparisons) changes in expression during progression of AMD. Values were normalized to control (MGS 1) samples. αA: αA-crystallin; GST: GST π. Data are mean ± SEM.

12 and inset). One major immune reaction corresponded with a spot migrating at a mass and pI that was consistent with theoretical values. The second major reaction, identified by MS analysis, decreased in density at late-stage AMD and migrated at a mass and pI that would be consistent with cleavage of an N-terminal mitochondrial signal sequence. Thus, these two major immunoreactive spots may represent mtHSP75 at different subcellular locations. Densitometry of 1-D Western blot immune reaction showed no significant change in mtHSP75 reaction with AMD (data not shown) and provides another example of an isoelectric variant exhibiting a different pattern of expression compared with the total protein population.

Discussion

In this study, we analyzed proteins from human donor eyes that were graded with the MGS for postmortem tissue. By using the MGS in conjunction with proteomics, we identified significant changes in human RPE proteins at distinct disease stages. Most of the changes occurred in early AMD and may correspond to causal mechanisms, whereas a small number changed late in the disease and may correspond to secondary consequences. These results can help direct the focus of future investigations by highlighting clinically relevant changes in RPE proteins and their corresponding cellular functions. Furthermore, because the MGS was derived from the AREDS classification system, our results are relevant for large clinical trials and epidemiologic studies that use the AREDS system. The direct relationship between the two classification systems should also facilitate translation of our findings at the molecular level to the clinical setting.

By combining high-resolution, quantitative 2-D gel analysis, mass spectrometry, and 1-D and 2-D Western blot analysis, this study extended a basic proteomic approach and highlighted several important considerations for future proteomic analyses. Because 2-D gel electrophoresis can separate proteins into individual isoelectric variants that potentially reflect functionally distinct subpopulations, it is important to determine the distribution of spots associated with specific proteins. This was especially relevant because, of the proteins detected by 2-D Western blot, only one (αA crystallin) migrated as a single spot. Proteins can resolve into multiple spots due to proteolytic processing, multiple isoforms, or changes in charge state resulting from posttranslational modifications including phosphorylation, deamidation, acetylation, glycation, and glutathionylation.[28–31] These posttranslational modifications can alter protein function. For example, glutathionylation of HSC70 converts this protein to an active chaperone.[32] The in vivo consequences of changing the distribution of isoelectric variants (e.g., HSP60 and GST-π) remain unclear but could affect subcellular localization and other functions regulated by posttranslational modification. Because most proteins migrated in multiple spots, we also used 1-D Western blot analysis to determine whether changes in individual isoelectric variants were representative of the entire protein population. Finally, when a mixture of proteins are found in a single spot, as observed for spot 5 containing both ATP synthase β and CRALBP, it is essential to examine individual protein constituents with alternative analytical techniques.

Although we identified several AMD-related changes, they probably reflect a conservative estimate of the total changes associated with AMD due to the technical constraints of our proteomic analysis. First, membrane proteins resolve poorly in the first dimension and are consequently underrepresented in the second dimension. Second, limiting the first dimension to a pH range of 5 to 8 provided the best resolution for the greatest number of spots but excluded proteins outside that range. Third, the detection limit for silver stained proteins and the sample size used in this study probably hindered our ability to detect changes in low-abundance proteins or changes smaller than a two-fold difference in expression.

Despite these caveats, our results provide the first direct evidence for decreased HSP expression (HSP70, HSC70, HSP60, αA crystallin) in early AMD. In general, HSPs can function as molecular chaperones to prevent cellular damage from unfolded proteins, including protein unfolding caused by oxidative damage.[33] More specifically, three of the HSPs identified by this study mediate the import and folding of mitochondrial proteins encoded by nuclear genes. After translation, mitochondrial proteins undergo HSP70-dependent transport to mitochondria.[34] mtHSP75 and HSP60 then mediate mitochondrial membrane trafficking and mitochondrial protein folding, respectively.[34,35] Decreased HSP expression may thus reflect impaired mitochondrial biogenesis in addition to impaired stress response mechanisms at early stages of AMD.

Several components of apoptotic signaling pathways (αA crystallin, VDAC1, HSP70, GST-π) also demonstrate early expression changes or changed linearly with AMD progression. For example, VDAC1 mediates the release of cytochrome *c* from mitochondria as part of the permeability transition pore.[36,37] αA-crystallin activates the anti-apoptotic Akt/protein kinase B pathway,[38] whereas HSP70 and GST-π inhibit proapoptotic c-Jun N-terminal kinase signaling.[39,40] GST-π also detoxifies endogenous and exogenous reactive electrophile groups,[41] and its upregulation may reflect a cellular response to increased oxidative stress. Because RPE cells are postmitotic and have a limited capacity for renewal, regulating apoptosis is essential for maintaining a functional RPE cell population and, consequently, preserving vision.

We also found late expression changes for two retinoid binding proteins (CRABP1 and CRALBP) that most likely reflect secondary disease processes. CRALBP binds 11-*cis* retinol as part of the visual cycle responsible for regenerating the rhodopsin chromophore.[42] CRABP1 regulates free retinoic acid levels by directly binding retinoic acid and increasing its metabolism, which is believed to affect retinoic acid signaling and homeostasis.[43,44] In turn, retinoic acid regulates RPE differentiation,[45] proliferation,[46] melanogenesis,[47] angiogenesis gene expression,[48,49] and expression of the visual cycle genes *RPE65* and *RLBP1*.[50] These findings suggest that late AMD is accompanied by the disruption of key retinoid-related functions in the RPE, although the relevance to AMD progression remains undefined.

In summary, the biochemical changes identified in this study represent novel contributions to understanding AMD pathophysiology and demonstrate the utility of proteomics for investigating human disease. More specifically, our proteomic examination of RPE protein from human donor eyes graded with the MGS has led to the identification of several critical proteins and potential pathways changing at early and late disease stages in human RPE, signifying both possible causal mechanisms and secondary consequences of AMD. Furthermore, our results are consistent with several hypotheses that identify oxidative stress, mitochondrial dysfunction, and RPE apoptosis as causal factors in AMD.[8–10] These mechanistic explanations of AMD pathogenesis share an underlying theme of cumulative damage to cellular components, reflecting its clinical presentation as an ageing disease. Our results also provide a basis for new directions in AMD research that may ultimately generate novel therapeutic strategies.

Acknowledgments

The authors thank the Minnesota Lions and Minnesota Lions Eye Bank personnel for their assistance in procuring eyes for this study; Kristin Pilon, Kathleen Lew, and the Mass Spectrometry Consortium for the Life Sciences (University of Minnesota) for technical assistance; and Cheryl Ethen for a thorough reading of the manuscript.

References

1. Leibowitz HM, Krueger DE, Maunder LR. The Framingham Eye Study monograph: an ophthalmological and epidemiological study of cataract, glaucoma, diabetic retinopathy, macular degeneration, and visual acuity in a general population of 2631 adults, 1973–1975. *Surv Ophthalmol*. 1980;24:335–610.
2. Klein R, Klein BE, Linton KL. Prevalence of age-related maculopathy. The Beaver Dam Eye Study. *Ophthalmology*. 1992;99:933–943.
3. U.S. Census Bureau. U.S. interim projections by age, sex, race, and hispanic origin. Washington DC: U.S. Bureau of the Census; 2004. http://www.census.gov/ipc/www/usinterimproj/.
4. Marmor MF, Wolfensberger TJ, eds. *The Retinal Pigment Epithelium.* New York: Oxford University Press; 1998.
5. Berger JW, Fine SL, Maguire MG, eds. *Age-Related Macular Degeneration.* St. Louis, MO: Mosby; 1999.
6. Curcio CA, Medeiros NE, Millican CL. The Alabama age-related macular degeneration grading system for donor eyes. *Invest Ophthalmol Vis Sci*. 1998;39:1085–1096.
7. Olsen TW, Feng X. The Minnesota Grading System of eye bank eyes for age-related macular degeneration. *Invest Ophthalmol Vis Sci*. 2004;45:4484–4490.
8. Dunaief JL, Dentchev T, Ying G, Milam AH. The role of apoptosis in age-related macular degeneration. *Arch Ophthalmol*. 2002;120:1435–1442.
9. Winkler BS, Boulton ME, Gottsch JD, Sternberg P. Oxidative damage and age-related macular degeneration. *Mol Vis*. 1999;5:32.
10. Liang FQ, Godley BF. Oxidative stress-induced mitochondrial DNA damage in human retinal pigment epithelial cells: a possible mechanism for RPE aging and age-related macular degeneration. *Exp Eye Res*. 2003;76:397–403.
11. Howes KA, Liu Y, Dunaief JL, et al. Receptor for advanced glycation end products and age-related macular degeneration. *Invest Ophthalmol Vis Sci*. 2004;45:3713–3720.
12. Kopitz J, Holz FG, Kaemmerer E, Schutt F. Lipids and lipid peroxidation products in the pathogenesis of age-related macular degeneration. *Biochimie* (*Paris*). 2004;86:825–831.
13. Crabb JW, Miyagi M, Gu X, et al. Drusen proteome analysis: an approach to the etiology of age-related macular degeneration. *Proc Natl Acad Sci USA*. 2002;99:14682–14687.
14. Hageman GS, Mullins RF. Molecular composition of drusen as related to substructural phenotype. *Mol Vis*. 1999;5:28.
15. Johnson LV, Leitner WP, Rivest AJ, Staples MK, Radeke MJ, Anderson DH. The Alzheimer's Aβ-peptide is deposited at sites of complement activation in pathologic deposits associated with aging and age-related macular degeneration. *Proc Natl Acad Sci USA*. 2002;99:11830–11835.
16. Edwards AO, Ritter R, Abel KJ, Manning A, Panhuysen C, Farrer LA. Complement factor H polymorphism and age-related macular degeneration. *Science*. 2005;308:421–424.
17. Hageman GS, Anderson DH, Johnson LV, et al. A common haplotype in the complement regulatory gene factor H (*HF1/CFH*) predisposes individuals to age-related macular degeneration. *Proc Natl Acad Sci USA*. 2005;102:7227–7232.
18. Haines JL, Hauser MA, Schmidt S, et al. Complement factor H variant increases the risk of age-related macular degeneration. *Science*. 2005;308:419–421.
19. Klein RJ, Zeiss C, Chew EY, et al. Complement factor H polymorphism in age-related macular degeneration. *Science*. 2005;308:385–389.
20. The Age-Related Eye Disease Study Group. The Age-Related Eye Disease Study system for classifying age-related macular degeneration from stereoscopic color fundus photographs: the Age-Related Eye Disease Study Report Number 6. *Am J Ophthalmol.* 2001;132:668–681.
21. Ethen CM, Feng X, Olsen TW, Ferrington DA. Declines in arrestin and rhodopsin in the macula with progression of age-related macular degeneration. *Invest Ophthalmol Vis Sci*. 2005;46:769–775.
22. Kapphahn RJ, Ethen CM, Peters EA, Higgins L, Ferrington DA. Modified αA crystallin in the retina: altered expression and truncation with aging. *Biochemistry*. 2003;42:15310–15325.
23. Laemmli UK. Cleavage of structural proteins during the assembly of the head of bacteriophage T4. *Nature*. 1970;277:680–685.
24. Ferrington DA, Krainev AG, Bigelow DJ. Altered turnover of calcium regulatory proteins of the sarcoplasmic reticulum in aged skeletal muscle. *J Biol Chem*. 1998;273:5885–5891.
25. Lehmann EL. *Testing Statistical Hypotheses.* 2nd ed. New York, NY: Wiley; 1986.
26. Friedman DS, Katz J, Bressler NM, Rahmani B, Tielsch JM. Racial differences in the prevalence of age-related macular degeneration: the Baltimore Eye Survey. *Ophthalmology*. 1999;106:1049–1055.
27. Beausoleil SA, Jedrychowski M, Schwartz D, et al. Large-scale characterization of HeLa cell nuclear phosphoproteins. *Proc Natl Acad Sci USA*. 2004;101:12130–12135.
28. Cherian M, Smith JB, Jiang XY, Abraham EC. Influence of protein-glutathione mixed disulfide on the chaperone-like function of alpha-crystallin. *J Biol Chem*. 1997;272:29099–29103.
29. Colvis, C, Garland, D. Posttranslational modification of human alphaA-crystallin: correlation with electrophoretic migration. *Arch Biochem Biophys*. 2002;397:319–323.
30. Hanson SRA, Hasan A, Smith DL, Smith JB. The major in vivo modifications of the human water-insoluble lens crystallins are disulfide bonds, deamidation, methionine oxidation and backbone cleavage. *Exp Eye Res*. 2000;71:195–207.
31. Ueda Y, Duncan MK, David LL. Lens proteomics: the accumulation of crystallin modifications in the mouse lens with age. *Invest Ophthalmol Vis Sci* 2002;43:205–215.
32. Hoppe G, Chai YG, Crabb JW, Sears J. Protein s-glutathionylation in retinal pigment epithelium converts heat shock protein 70 to an active chaperone. *Exp Eye Res*. 2004;78:1085–1092.
33. Martindale JL, Holbrook NJ. Cellular response to oxidative stress: Signaling for suicide and survival. *J Cell Physiol*. 2002;192:1–15.
34. Ryan MT, Pfanner N. Hsp70 proteins in protein translocation. *Adv Protein Chem*. 2001;59:223–242.
35. Voos W, Rottgers K. Molecular chaperones as essential mediators of mitochondrial biogenesis. *Biochim Biophys Acta*. 2002;1592:51–62.
36. Crompton C. The mitochondrial permeability transition pore and its role in cell death. *Biochem J*. 1999;341:233–249.
37. Zalk R, Israelson A, Garty ES, Azoulay-Zohar H, Shoshan-Barmatz V. Oligomeric states of the voltage-dependent anion channel and cytochrome c release from mitochondria. *Biochem J*. 2005;386:73–83.
38. Liu JP, Schlosser R, Ma WY, et al. Human αA- and αB-crystallins prevent UVA-induced apoptosis through regulation of PKCα, RAF/MEK/ERK and AKT signaling pathways. *Exp Eye Res*. 2004;79:393–403.
39. Beere HM. 'The stress of dying': the role of heat shock proteins in the regulation of apoptosis. *J Cell Sci*. 2004;117:2641–2651.
40. Wang T, Arifoglu P, Ronai MZ, Tew KD. Glutathione *S*-transferase P1–1 (GSTP1–1) inhibits c-Jun N-terminal kinase (JNK1) signaling through interaction with the C terminus. *J Biol Chem*. 2001;276:20999–21003.
41. Ralat LA, Colman RF. Glutathione *S*-transferase Pi has at least three distinguishable xenobiotic substrate sites close to its glutathione-binding site. *J Biol Chem*. 2004;279:50204–50213.
42. Thompson DA, Gal A. Vitamin A metabolism in the retinal pigment epithelium: genes, mutations, and diseases. *Prog Retin Eye Res*. 2003;22:683–703.
43. Napoli JL. Biochemical pathways of retinoid transport, metabolism, and signal transduction. *Clin Immunol Immunopathol*. 1996;80:S52–S62.
44. Won JY, Nam E, Yoo SJ, et al. The effect of cellular retinoic acid binding protein-I expression on the CYP26-mediated catabolism of

all-*trans* retinoic acid and cell proliferation in head and neck squamous cell carcinoma. *Metabolism*. 2004;53:1007–1012.
45. Janssen JJ, Kuhlmann ED, van Vugt AH, et al. Retinoic acid delays transcription of human retinal pigment neuroepithelium marker genes in ARPE-19 cells. *Neuroreport*. 2000;11:1571–1579.
46. Yasunari T, Yanagihara N, Komatsu T, et al. Effect of retinoic acid on proliferation and polyamine metabolism in cultured bovine retinal pigment epithelial cells. *Ophthalmic Res*. 1999; 31:24–32.
47. Kishi H, Kuroda E, Mishima HK, Yamashita U. Role of TGF-β in the retinoic acid-induced inhibition of proliferation and melanin synthesis in chick retinal pigment epithelial cells *in vitro*. *Cell Biol Int*. 2001;25:1125–1129.
48. Tombran-Tink J, Lara N, Apricio SE, et al. Retinoic acid and dexamethasone regulate the expression of PEDF in retinal and endothelial cells. *Exp Eye Res*. 2004;78:945–955.
49. Uchida H, Hayashi H, Kuroki M, et al. Vitamin A up-regulates the expression of thrombospondin-1 and pigment epithelium-derived factor in retinal pigment epithelial cells. *Exp Eye Res*. 2005;80:23–30.
50. Mori M, Metzger D, Picaud S, et al. Retinal dystrophy resulting from ablation of RXRα in the mouse retinal pigment epithelium. *Am J Pathol*. 2004;164:701–710.

E R R A T A

***Erratum in*:** "Vascular Damage in a Mouse Model of Diabetic Retinopathy: Relation to Neuronal and Glial Changes" by Feit-Leichman et al. (*Invest Ophthalmol Vis Sci*. 2005;46: 4281–4287).

In the second paragraph of the Discussion, on page 4285, Reference #18 is cited incorrectly. The correct reference is Barber AJ, Antonetti DA, Kern TS, et al. The $Ins2^{Akita}$ mouse as a model of early retinal complications in diabetes. *Invest Ophthalmol Vis Sci*. 2005;46:2210–2218.

***Erratum in*:** "Effects of Sustained Hyperoxia on Revascularization in Experimental Retinopathy of Prematurity" by Gu et al. (*Invest Ophthalmol Vis Sci*. 2002;43:496–502).

The correct spelling of the third author's name is Mohamed Al-Shabrawey.

***Erratum in*:** "Development of a Questionnaire to Assess Vision Problems under Low Luminance in Age-Related Maculopathy" by Owsley et al. (*Invest Ophthalmol Vis Sci*. 2006;47: 528–535).

In the footnote to Table 4, item 6 was left out of the extreme lighting list. The footnote should read as follows:

Items in each subscale: driving (24, 25, 26, 27, 28), extreme lighting (1, 2, 3, 4, 5, 6, 7, 8), mobility (9, 10, 11, 12, 13, 14), emotional distress (29, 30, 31, 32), general dim lighting (15, 16, 17, 18, 19, 20) and peripheral vision (21, 22, 23).